Supporting Information

In-situ sulfidation induced Bi_2S_3 heterogeneous phase on $CuBi_2O_4$ for boosting photoelectrochemical ammonia production

Xiaohong Wang,[a] Pengpeng Yang,[a] Zhonghua You,[a] Longbao Yu,[a] Chen Hao,[a] Xiaoqi Fu,[a] Hongye Bai,[a*] Guohai Xu,[c*] Weiqiang Fan[a,b*]

[a] *School of Chemistry and Chemical Engineering, Jiangsu University, Zhenjiang, 212013, PR China.*

[b] *Key Laboratory of Green Extraction and Efficient Utilization of Light Rare-Earth Resources (Ministry of Education), Baotou, 014010, PR China.*

[c] *Key Laboratory of Jiangxi University for Functional Materials Chemistry, School of Chemistry and Chemical Engineering, Gannan Normal University, Ganzhou, Jiangxi 341000, PR China.*

E-mail: bhy198412@163.com, xuguohai@gnnu.edu.cn, fwq4993329@ujs.edu.cn

1. Experimental component

1.1 Chemical reagents

Copper nitrate trihydrate ($Cu(NO_3)_2·3H_2O$), bismuth nitrate pentahydrate ($Bi(NO_3)_3·5H_2O$), concentrated nitric acid, thioacetamide (C_2H_5NS), anhydrous sodium sulfate (Na_2SO_4), potassium sodium tartrate ($NaKC_4H_4O_6$), all drugs and reagents are purchased from Sinopharm Group Chemical Reagents Co., LTD. Disodium hydrogen phosphate (Na_2HPO_4) and Nessler's reagent (K_2HgI_4) were obtained from McLean. Fluorine-doped tin oxide conductive glass (FTO 14 Ω) was purchased from Wuhan Jingge Solar Technology Co. The products and reagents are analytically pure and do not require further purification for use.

1.2. Synthesis of $CuBi_2O_4$

Firstly, 2.5 mmol of $Cu(NO_3)_2·3H_2O$ and 5 mmol of $Bi(NO_3)_3·5H_2O$ were weighed and dissolved in a 1% HNO_3. The solution was stirred by ultrasonication for 30 min until the solution became transparent. In the electrochemical deposition process, Ag/AgCl was used as the reference electrode, Pt as the counter electrode and FTO as the working electrode, and the above solution was used as the electrolyte. Electrodeposition was carried out at a constant potential of -0.5 V by using a constant potentiostat (model 660). Then, the black Cu-Bi alloy film was obtained and dried in an oven at 60 °C for 10 min. Finally, the Cu-Bi alloy film was annealed in air at 450 °C for 4 h and transformed in $CuBi_2O_4$ photocathode.

1.3. Synthesis of $CuBi_2O_4/Bi_2S_3$

The in-situ heterojunction of $CuBi_2O_4/Bi_2S_3$ was synthesized through a one-step hydrothermal approach. Initially, 7.5 mmol of thioacetamide(C_2H_5NS) were dissolved in 40 mL of deionized water. The solution was stirred magnetically for 10 min to ensure complete dissolution and uniform mixing. Subsequently, a $CuBi_2O_4$-loaded

FTO substrate was placed into a Teflon-lined autoclave, and 25 mL of the prepared solution was added. Then, the stainless-steel autoclave was sealed and maintained at 180°C in an oven for 10 h. After the heating process was completed, the sample was cooled naturally to room temperature and was subsequently rinsed with deionized water to remove any surface residues. Finally, the sample was dried in an oven to obtain the $CuBi_2O_4/Bi_2S_3$ composite.

1.4. Characterization of the photocathode

The micro-morphology of the catalysts was analyzed using field emission scanning electron microscopy (FESEM, Apreo SHiVac, 3 kV) and transmission electron microscopy (TEM, Tecnai G2 F20 S-Twin electron microscope (FEI Co.)). Energy dispersive spectroscopy (EDS, XMAX 50) showed the distribution of elements in the samples. The crystal structure of the samples was studied by X-ray diffraction (XRD, Bruker D8 ADVANCE, Cu Kα). The elemental composition and valence states of the catalysts were characterized by X-ray photoelectron spectroscopy (XPS, Thermos Fisher Scientific, Escalab 250 Xi, Al Ka). The UV-Vis absorption spectra of the solids were tested by UV-3600 Plus instrument (Shimadzu, Japan). The absorbance of the reaction solutions was tested using a UV-Vis spectrophotometer (UV-vis 2550 Shimadzu).

1.5. PEC Measurement

The PEC performance of the synthesized photocathode was evaluated at room temperature using a standard three-electrode setup and an electrochemical workstation (CHI 614). A sample of 1 cm^2 served as the working electrode, with Ag/AgCl as the reference electrode and a Pt sheet of 1 cm^2 as the counter electrode. The H-type electrolyzer was employed as PEC NIRR device, which was separated into anode and cathode chambers by a Nifion proton exchange membrane. Before the reaction, Argon

(Ar) was continuously purged into the cathode chamber to eliminate the interference of O_2 and N_2 in the air. The 0.5 M Na_2SO_4 aqueous solution was used as the test electrolyte, and a Na_2SO_4 solution containing $NaNO_3$ (150 μg·mL^{-1}) was used as the reaction solution. The reduction process occurred in the cathode chamber, and a 300 W xenon lamp (100 mW cm^{-2}, luminous spectral range: 350−1100 nm, Beijing CEL-S500) served as the illumination source, irradiating the working electrode throughout the reduction process. Linear sweep voltammetry (LSV) tests were conducted with a scan rate of 50 mV/s. The electrochemical double layer capacitance (C_{dl}) was assessed using cyclic voltammetry (CV) at scan rates ranging from 20 mV/s to 100 mV/s. All electrode potentials were calculated using the Nernst equation:

$$E\ (RHE) = E\ (Ag/AgCl) + 0.059\,pH + 0.197$$

1.6. Analytical methods

The detection of NH_3: The yield of NH_3 is analyzed spectrophotometrically using Nessler reagent. Ten milliliters of the reaction electrolyte was taken and 0.2 mL potassium sodium tartrate ($KNaC_4H_6O_6$-H_2O, concentration 0.5 g/mL) solution and 0.2 mL of Nath's reagent were added, and stand for 10 minutes. Subsequently, the absorbance of the mixed solution was measured at 425 nm using UV-Vis spectrophotometry. To establish the standard curve, different concentrations of ammonium chloride (NH_4Cl) solution were used for linear fitting, and the relationship equation between absorbance and NH_4Cl concentration was obtained as $y = 0.20756x + 0.00637$, and the relevant data are shown in Fig. S18.

The detection of NO_2^-: First, configure the chromogenic agent. 4 g p-aminobenzenesulfonamide was accurately weighed and added to a mixed solution consisting of 50 mL H_2O and 10 mL phosphoric acid. Next, 0.2 g N-(1-naphthyl)-ethylenediamine dihydrochloride was added to this solution and stirred well. The

solution was transferred to a 100 mL volumetric flask and diluted with distilled water. Remove 10 mL of the reaction electrolyte and add 0.8 mL chromogenic agent to it. After mixing and standing for 10 min, the absorbance of the solution was measured at 540 nm by UV-Vis spectrophotometry. According to the measurement results of different concentrations of standard solutions, the standard curve was plotted, and the linear equation obtained was $y = 0.78898x - 0.01239$, and the relevant data were shown in Fig. S19.

The detection of NO_3^-: First, dilute 2.0 mL of reaction solution with deionized water to 20 mL. Add 0.4 mL 1 M HCl solution and 1.2 mL sulfamic acid solution (0.8 wt %) to the solution. The solution was mixed and stood for 10 minutes. The absorbance of the solution was then measured by UV-Vis spectrophotometry at 225 nm and 275 nm. The final absorbance of NO_3^- was calculated according to the following equation: $A = A_{225\ nm} - 2A_{275\ nm}$. Standard curves were obtained for different concentrations of $NaNO_3$ solutions, and the corresponding absorbance versus the concentration of $NaNO_3$ was given by $y = 0.0331x - 0.01132$, as shown in Fig. S20.

The H radical trapping experiment: The generation of H radicals was further examined using electron paramagnetic resonance (EPR) spectroscopy with 5,5-dimethyl-1-pyrroline N-oxide (DMPO) as the spin-trapping agent. For the measurements, the $CuBi_2O_4/Bi_2S_3$ sample was placed in the cathodic chamber containing 50 mL Na_2SO_4 solution (0.5 M), both with and without 150 ppm NO_3^-. Photoelectrochemical nitrogen reduction reaction (PEC NIRR) was conducted for 10 min under optimized conditions (-0.6 V vs. Ag/AgCl applied potential and 100 mW cm^{-2} xenon lamp illumination). Subsequently, 50 μL of the reaction solution was extracted and mixed with 50 μL DMPO. The resulting mixture was promptly

analyzed by EPR spectroscopy.

1.7. Computational methods

The yield rate (aq) is calculated as follows:

$$V_{NH_3} = (C_{NH_3} \times V) / (S \times t)$$

$$V_{NO_2^-} = (C_{NO_2^-} \times V) / (S \times t)$$

The conversion rate of NO_3^- is as follows:

$$NO_3^- \text{ conversion} = \Delta C_{NO_3^-} / C_0 \times 100\%$$

The formula for NH_3 selectivity (aq) is as follows:

$$S_{NH_3} = C_{NH_3} / \Delta C_{NO_3^-} \times 100\%$$

C_{NH_3} and $C_{NO_2^-}$ represent NH_3 and NO_2^- concentrations ($\mu g \cdot mL^{-1}$), V stands for electrolytic liquid volume (mL), S is the reaction area of the photoelectrode (cm^2); t stands for reaction time (h); C_0 is the initial concentration of NO_3^-, ΔCNO_3^- represents the concentration difference of NO_3^- before and after the reaction.

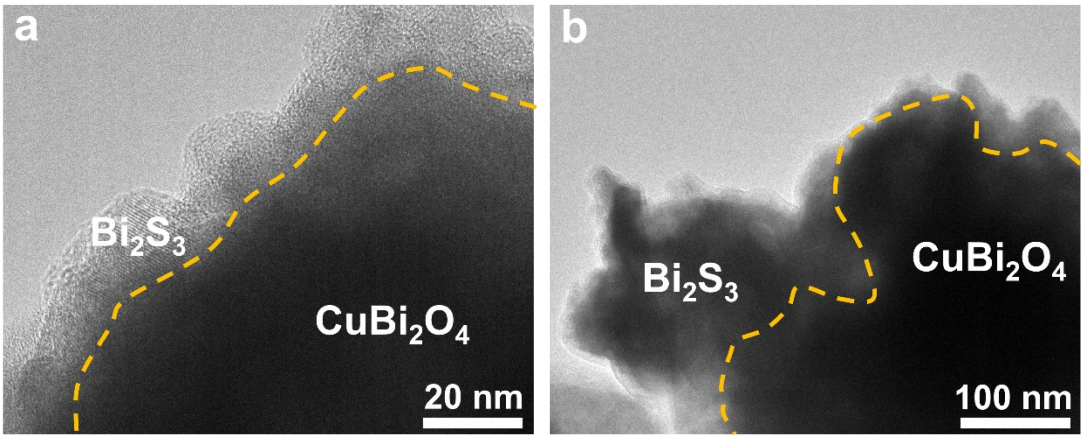

Fig. S1 TEM of $CuBi_2O_4/Bi_2S_3$.

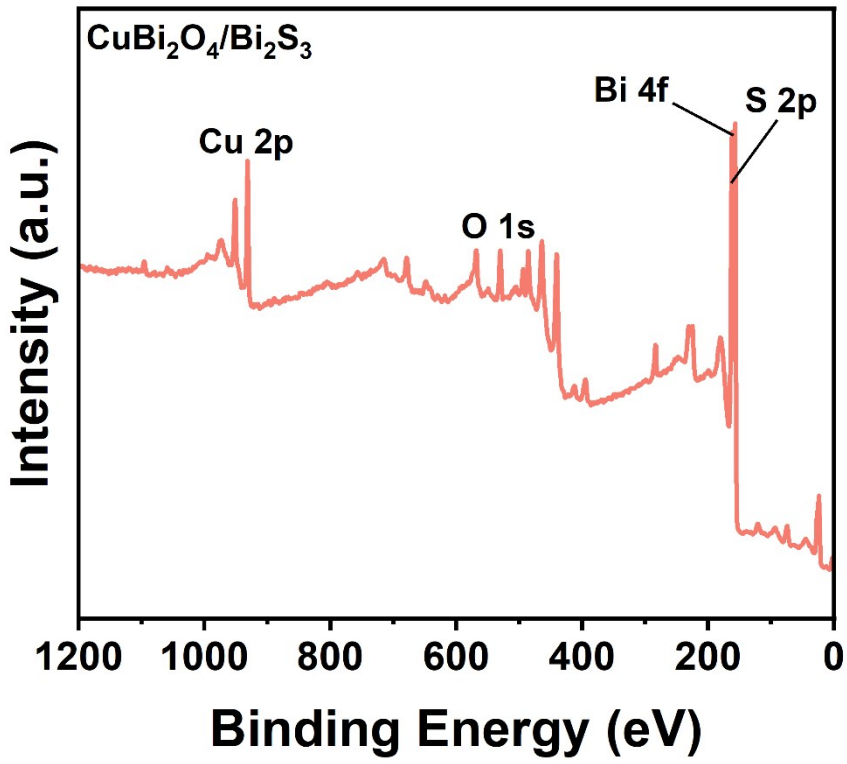

Fig. S2 XPS spectra of $CuBi_2O_4/Bi_2S_3$.

Table S1. The relative ratios of the surface concentration of O_v based on XPS analysis.

	$CuBi_2O_4$	$CuBi_2O_4/Bi_2S_3$
O_{latt}	40807.72	5643.41
O_v	18321.77	11530.75
O_{ads}	26166.37	6366.2
[Ov/O]%	21.48	48.98

O: Photoelectron peak area of O_{latt}, O_{ads} and O_v. O_v: photoelectron peak area of O_v.

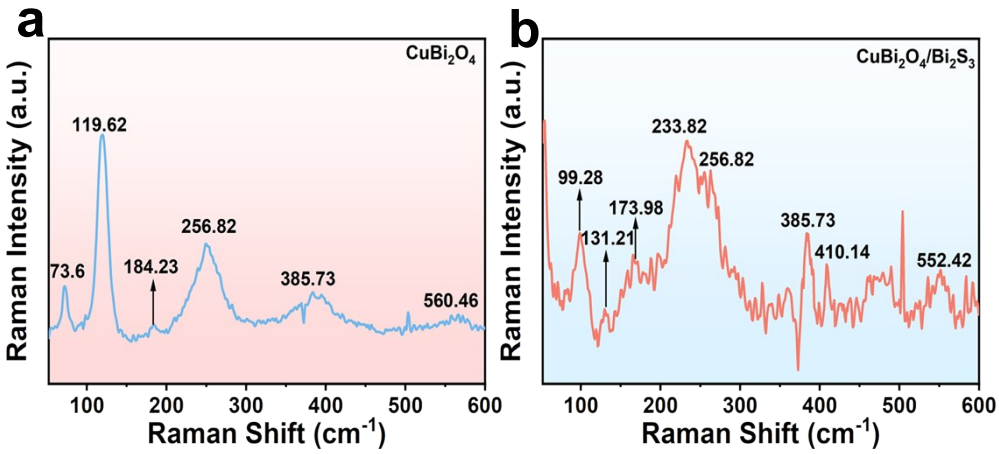

Fig. S3 Raman spectra of $CuBi_2O_4$ (a) and $CuBi_2O_4/Bi_2S_3$ (b).

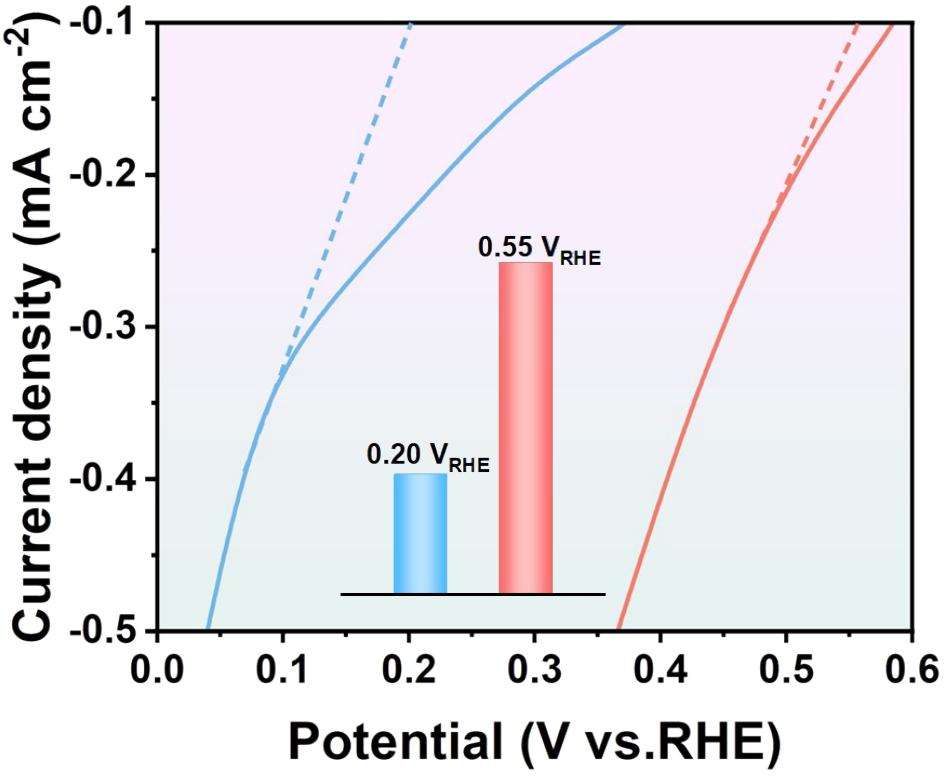

Fig. S4 Onset Potential (V_{on}) of $CuBi_2O_4$ and $CuBi_2O_4/Bi_2S_3$.

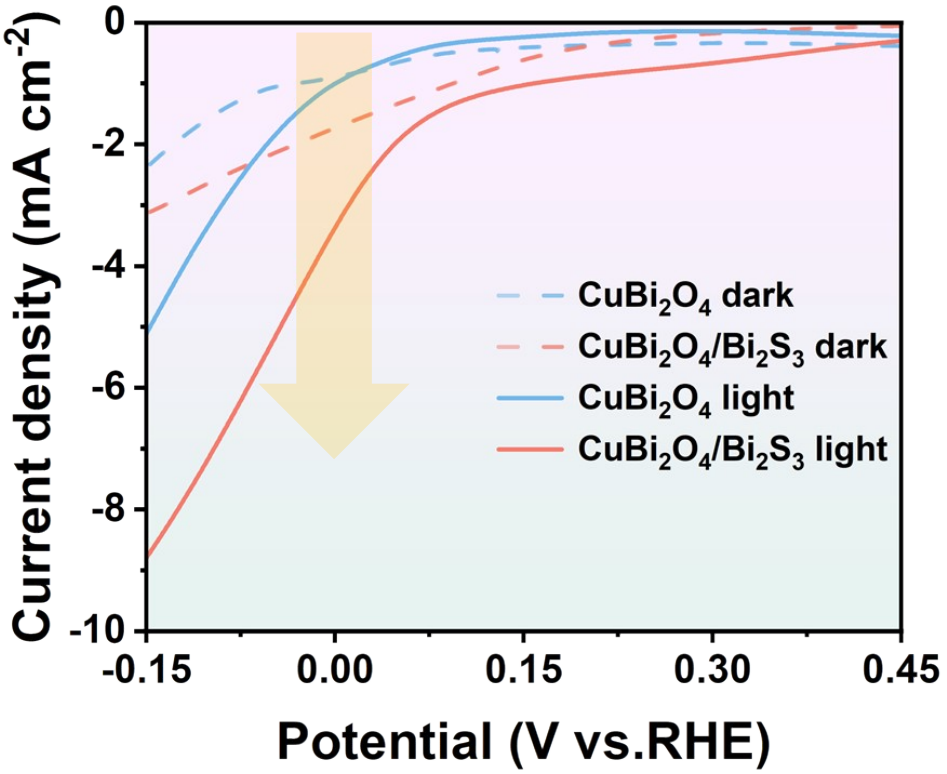

Fig. S5 LSV curves with and without light addition of $CuBi_2O_4$ and $CuBi_2O_4/Bi_2S_3$.

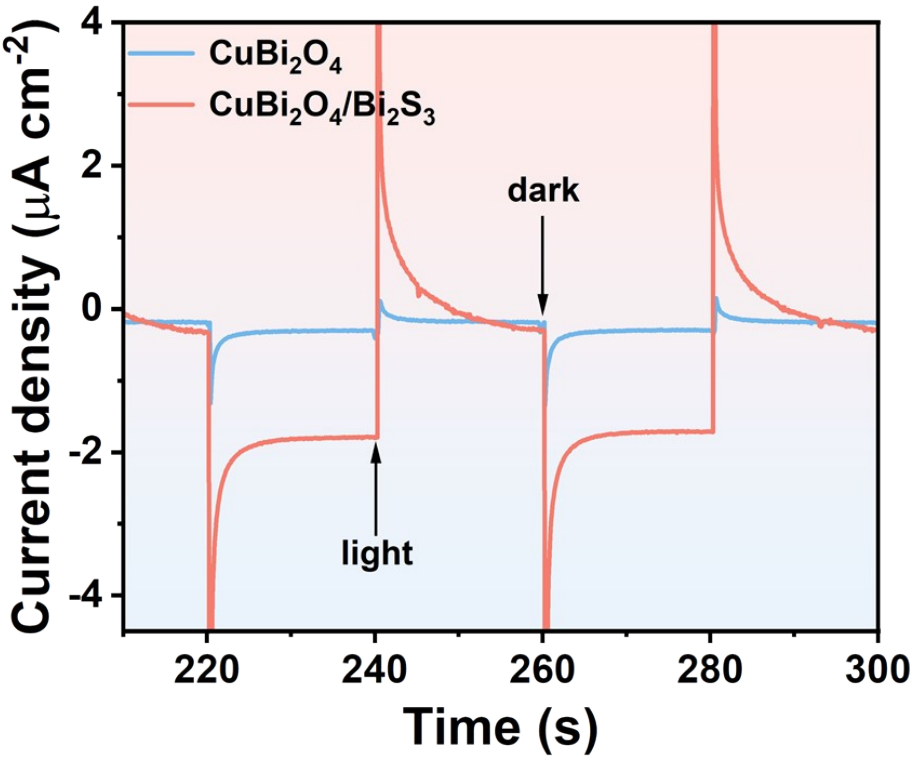

Fig. S6 Transient photocurrent curves under repeated light/dark cycles.

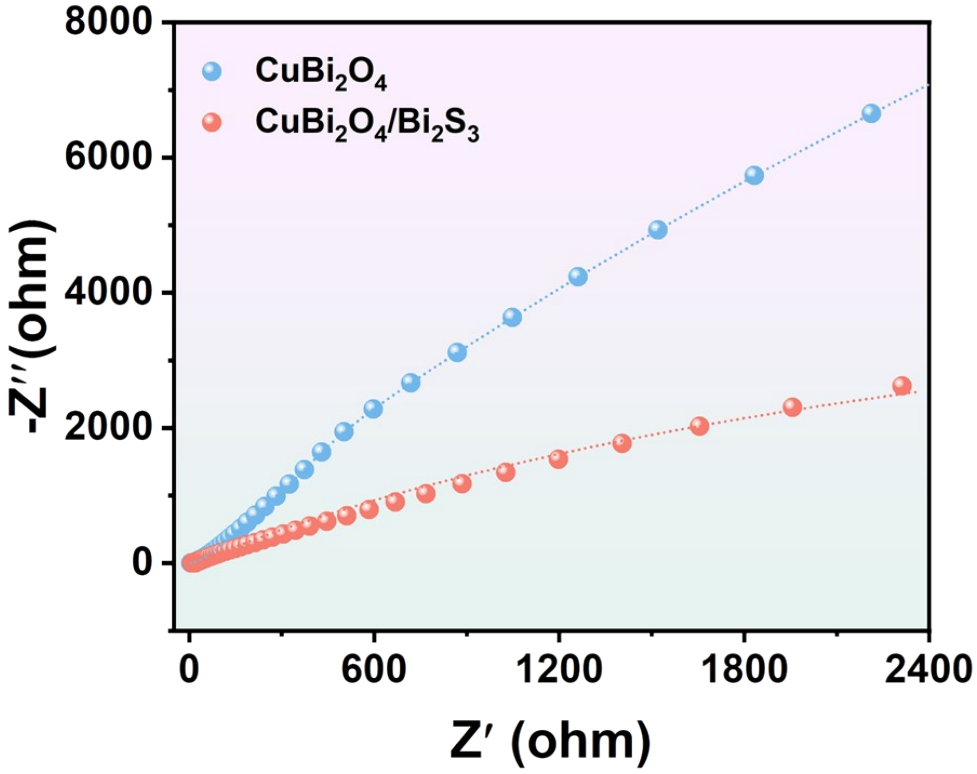

Fig. S7 PEIS plots of $CuBi_2O_4$ and $CuBi_2O_4/Bi_2S_3$.

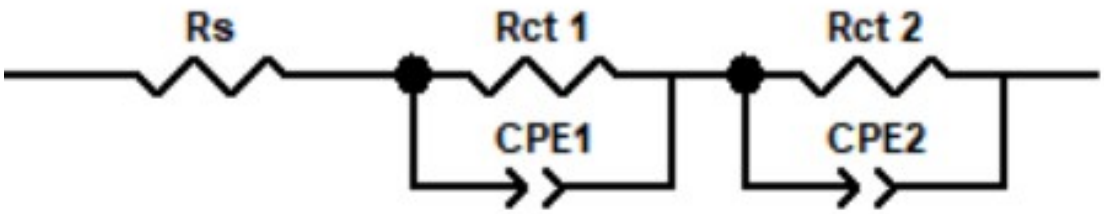

Fig. S8 Equivalent circuit diagram of the photoelectrode.

Table S2. Samples of R_{ct} 1 and R_{ct} 2 values.

Sample	Rct 1($\Omega \cdot cm^2$)	Rct 2($\Omega \cdot cm^2$)
$CuBi_2O_4$	10.64	60752
$CuBi_2O_4/Bi_2S_3$	6.794	10809

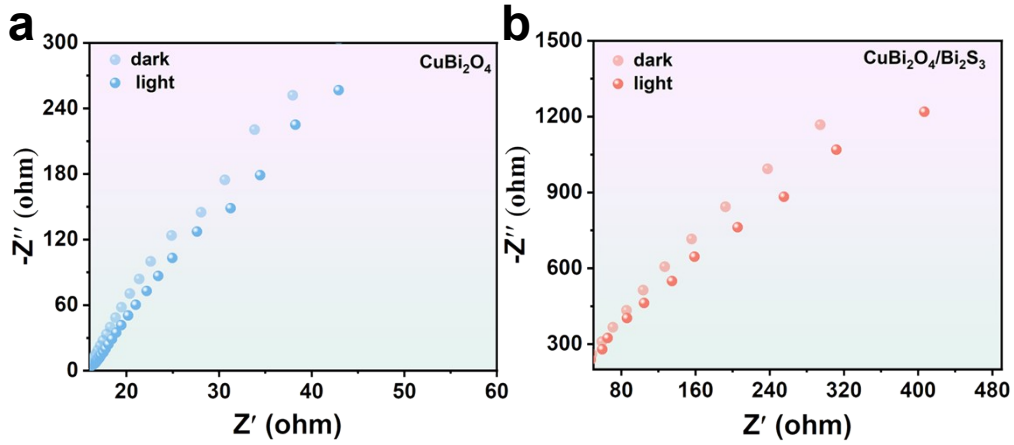

Fig. S9 PEIS plots of $CuBi_2O_4$ and $CuBi_2O_4/Bi_2S_3$ in dark and light conditions.

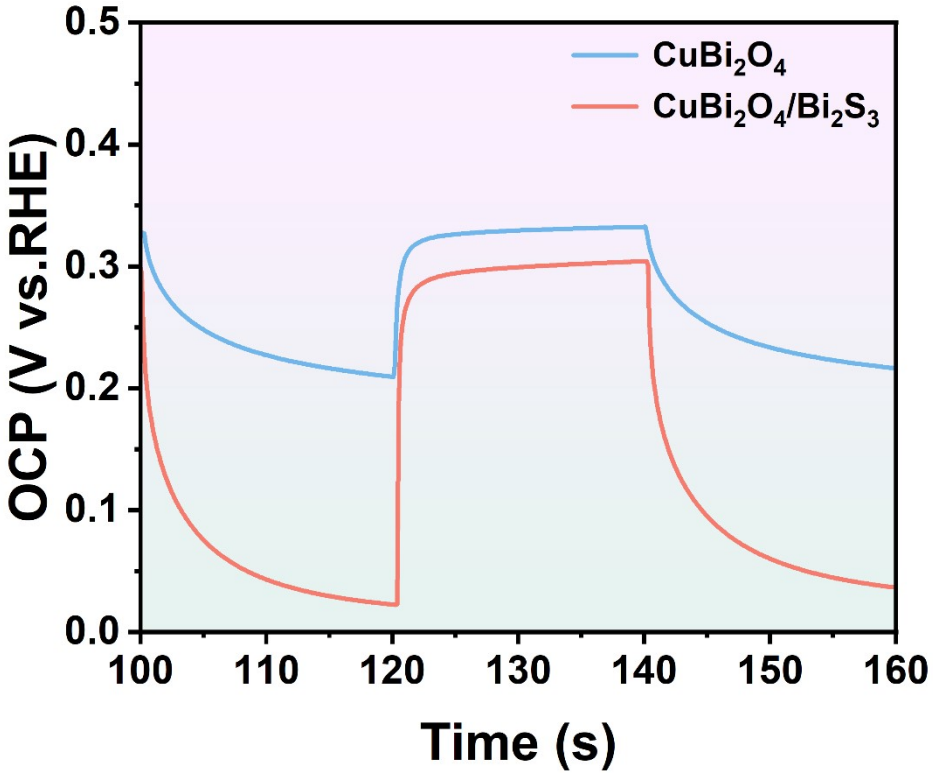

Fig. S10 OCP curves of the $CuBi_2O_4$ and $CuBi_2O_4/Bi_2S_3$.

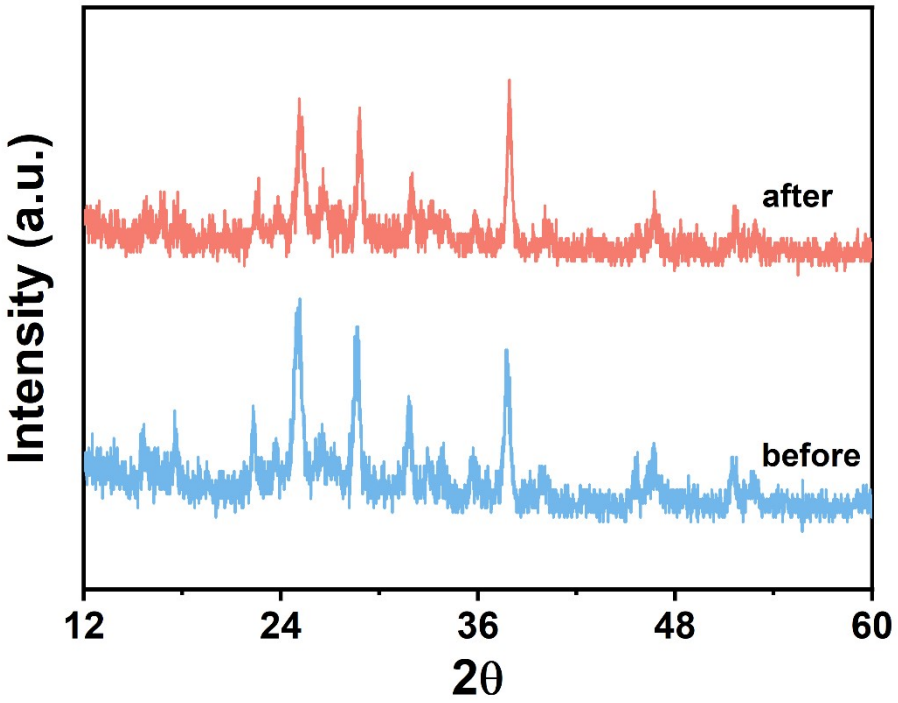

Fig. S11 Comparison of XRD before and after reaction of $CuBi_2O_4/Bi_2S_3$.

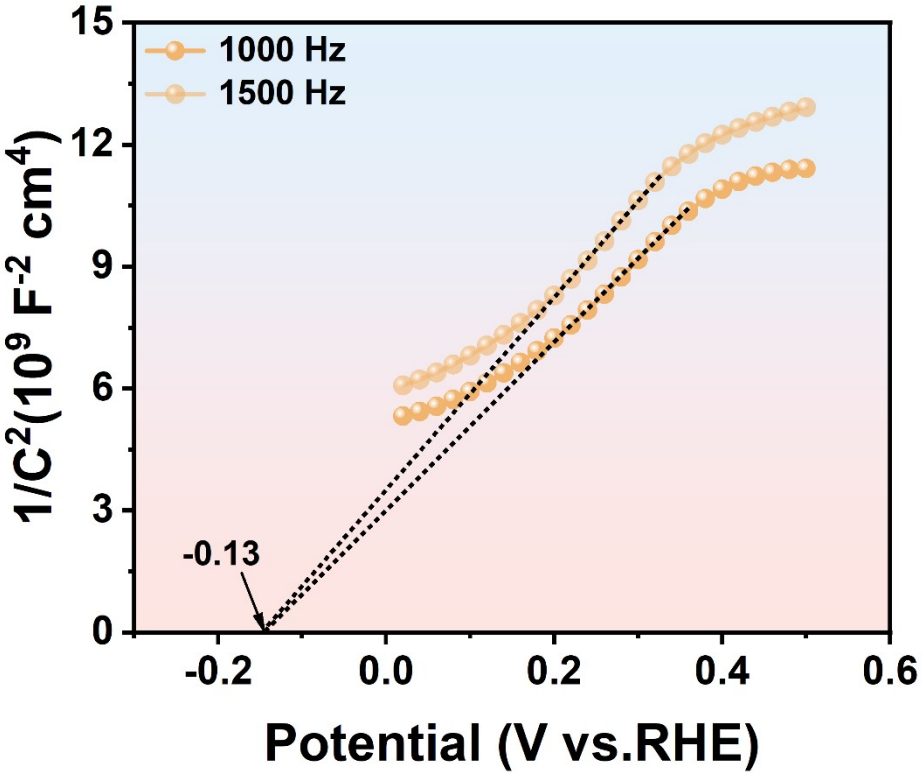

Fig. S12 Mott-schottky diagram of Bi_2S_3.

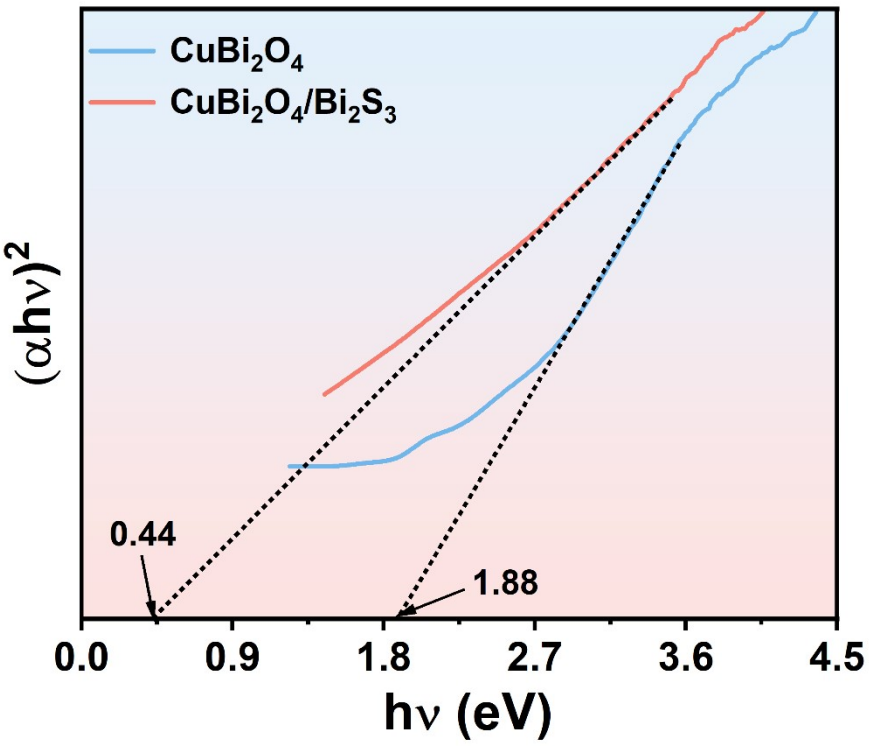

Fig. S13 Tauc plot of $CuBi_2O_4$ and $CuBi_2O_4/Bi_2S_3$.

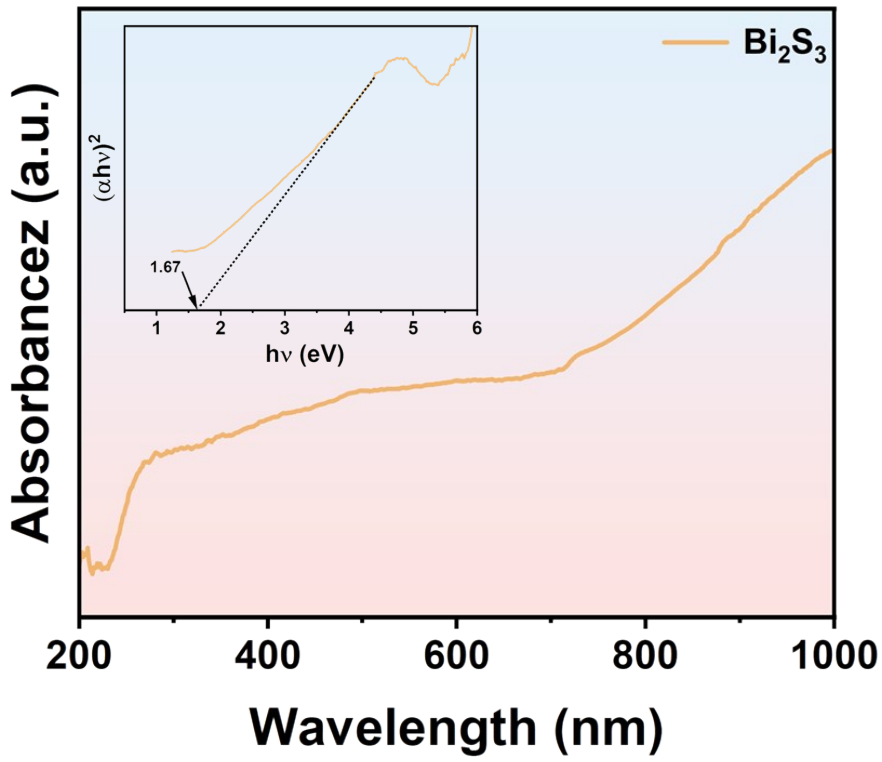

Fig. S14 UV-vis absorption spectra and tauc plot of Bi_2S_3.

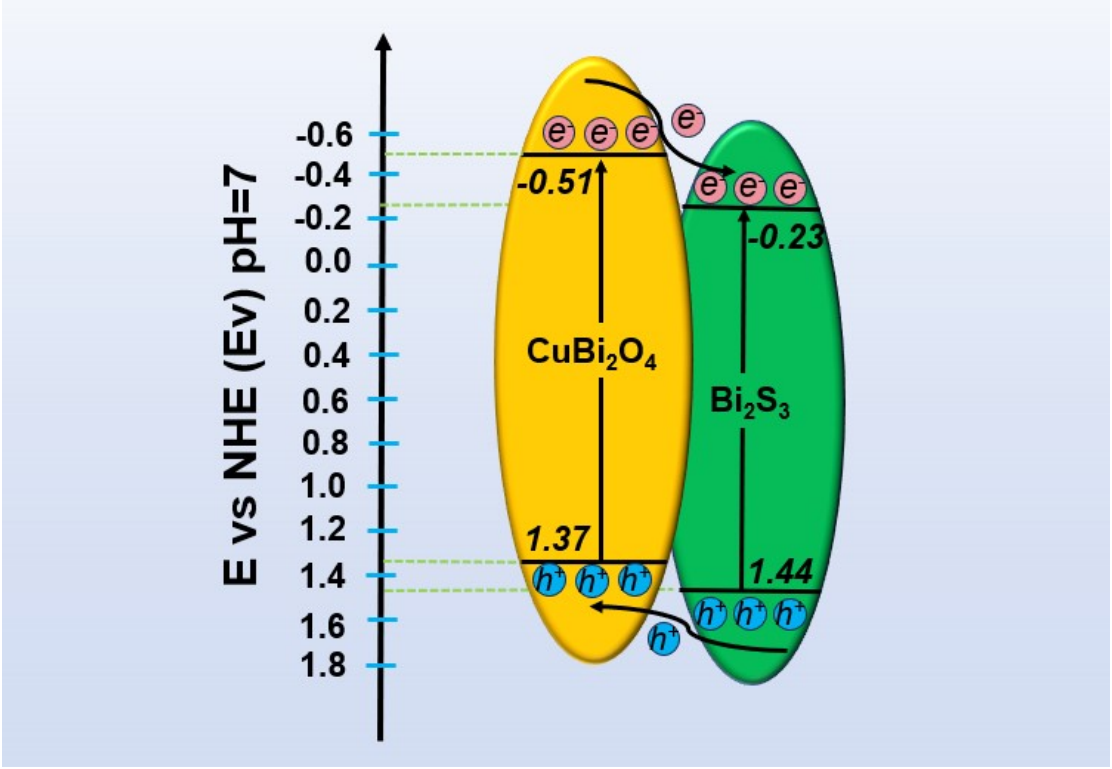

Fig. S15 Energy level diagram of $CuBi_2O_4$ and Bi_2S_3.

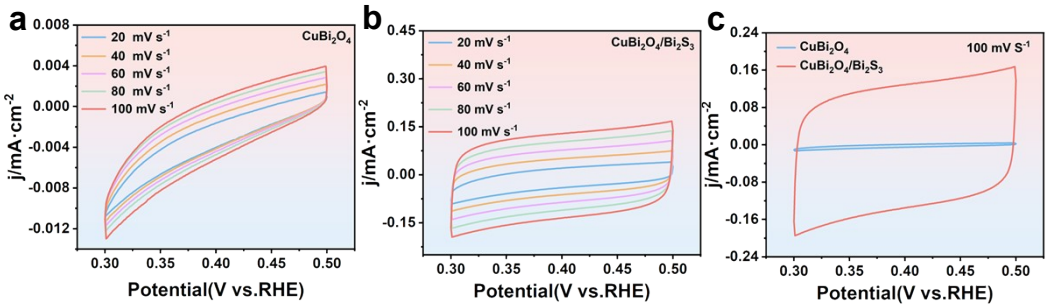

Fig. S16 CV curves at different scan rates (20 mV/s-100 mV/s) of (a) $CuBi_2O_4$, (b) $CuBi_2O_4/Bi_2S_3$. (c). CV curves at 100 mV/s of $CuBi_2O_4$ and $CuBi_2O_4/Bi_2S_3$.

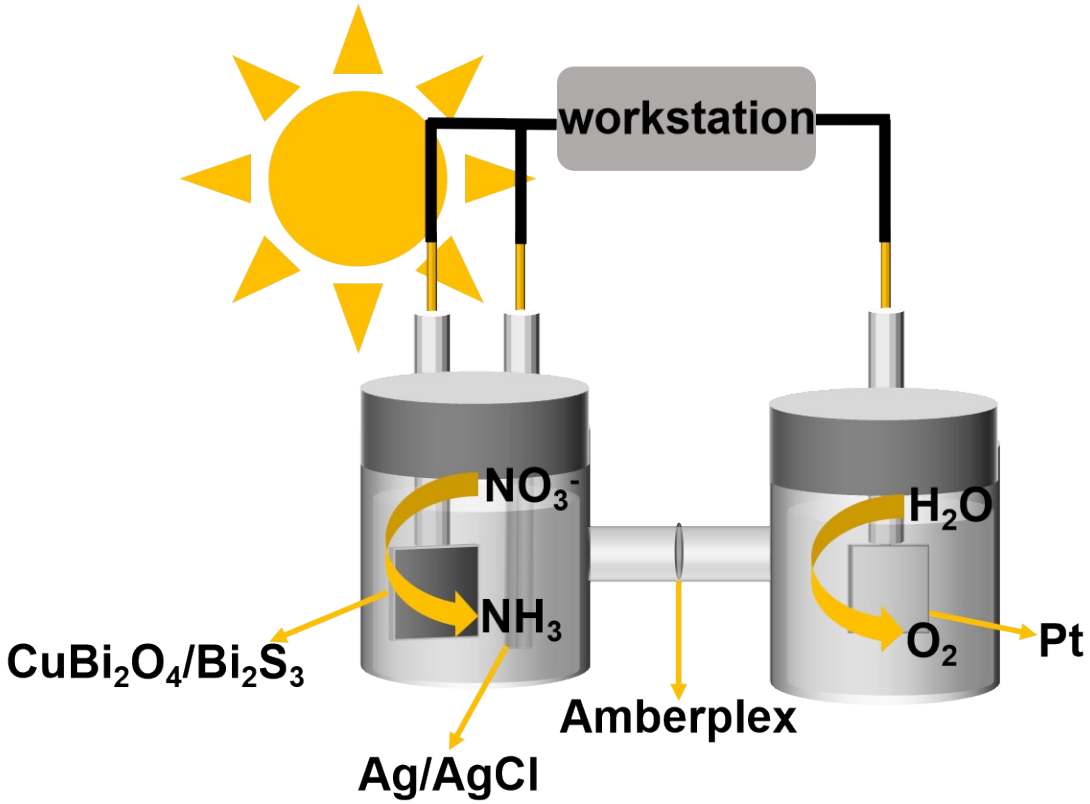

Fig. S17 Photoelectrochemical reaction unit for ammonia production.

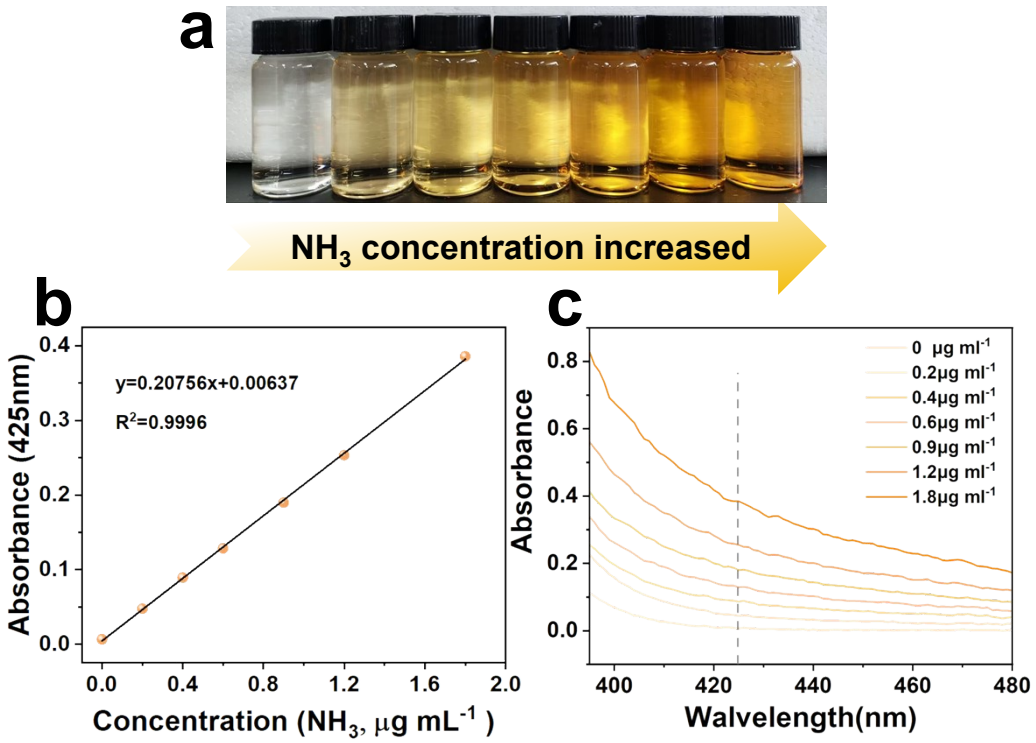

Fig. S18 (a) Digital photographs of the reaction of NH_3 at different concentrations; (b) Linear fit curve of absorbance at 425 nm at different concentrations. (c) UV-vis spectra of NH_3 at different concentrations;

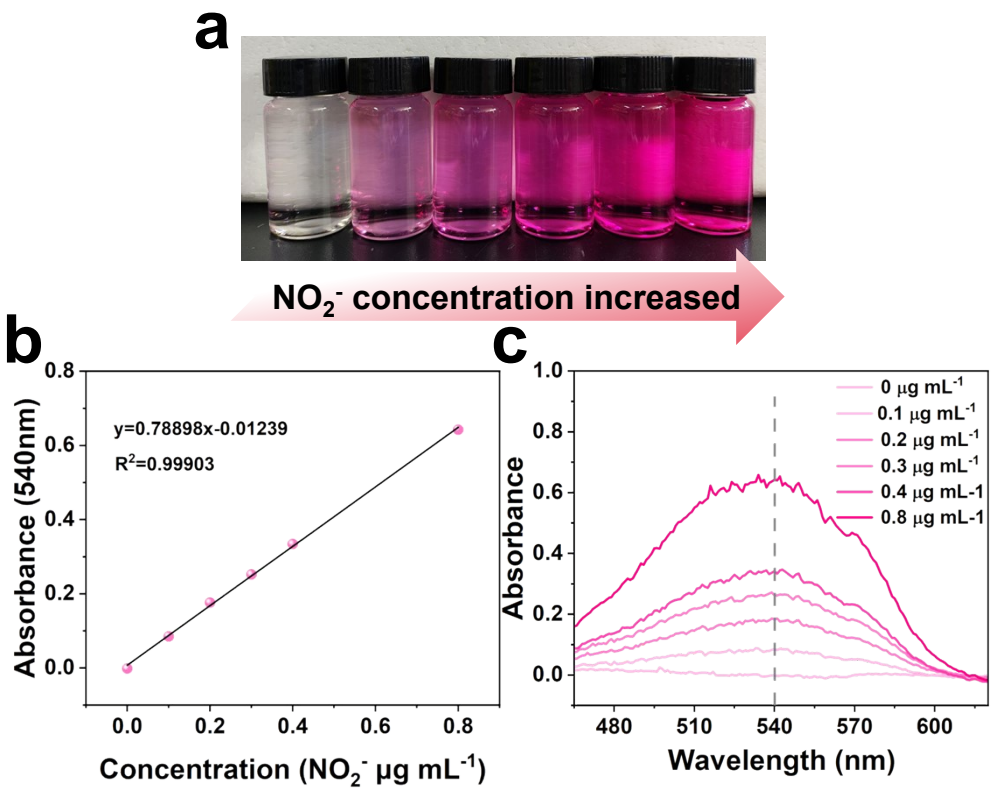

Fig. S19 (a) Digital photographs of the reaction of NO_2^- at different concentrations; (b) Linear fit curve of absorbance at 540 nm at different concentrations. (c) UV-vis spectra of NO_2^- at different concentrations;

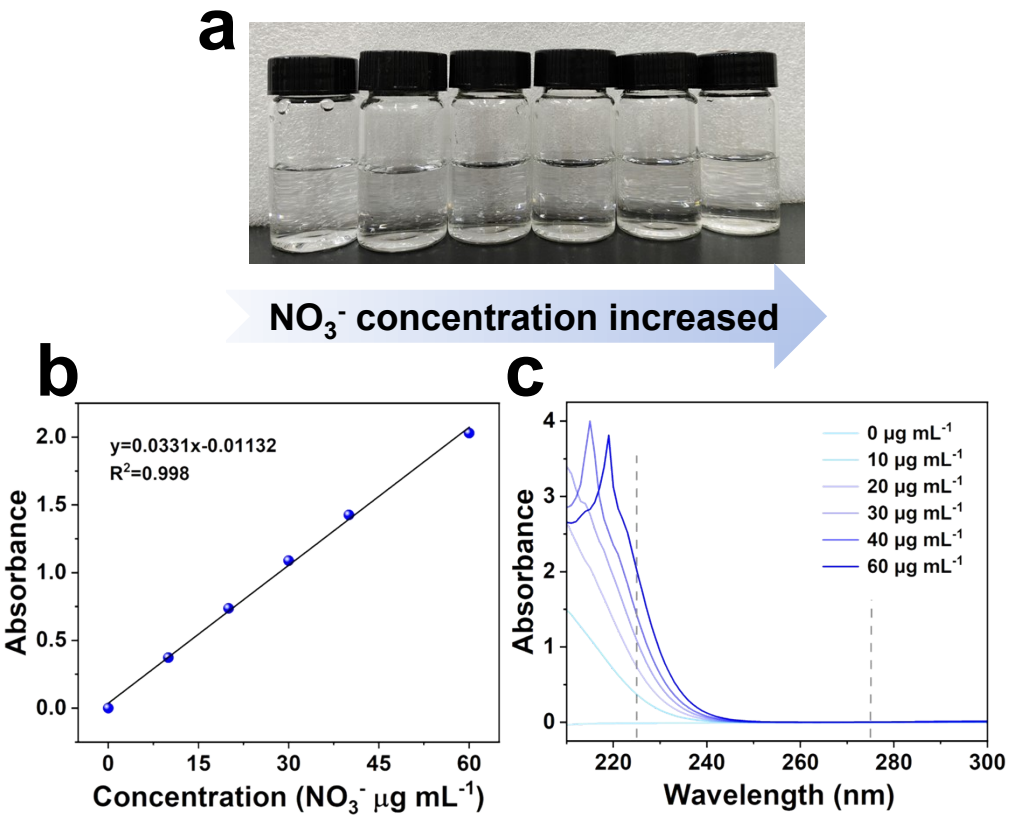

Fig. S20 (a) Digital photographs of the reaction of NO_3^- at different concentrations; (b) Linear fit curve of absorbance at different concentrations. (c) UV-vis spectra of NO_3^- at different concentrations;

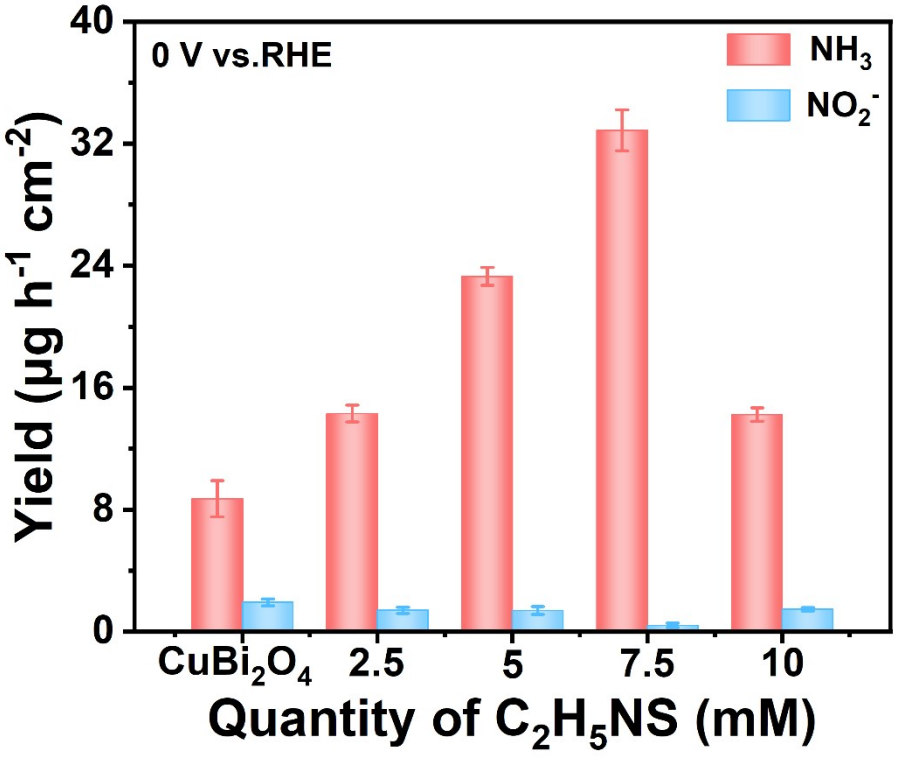

Fig. S21 NH_3 and NO_2^- yield under different quantity of sulfur sources.

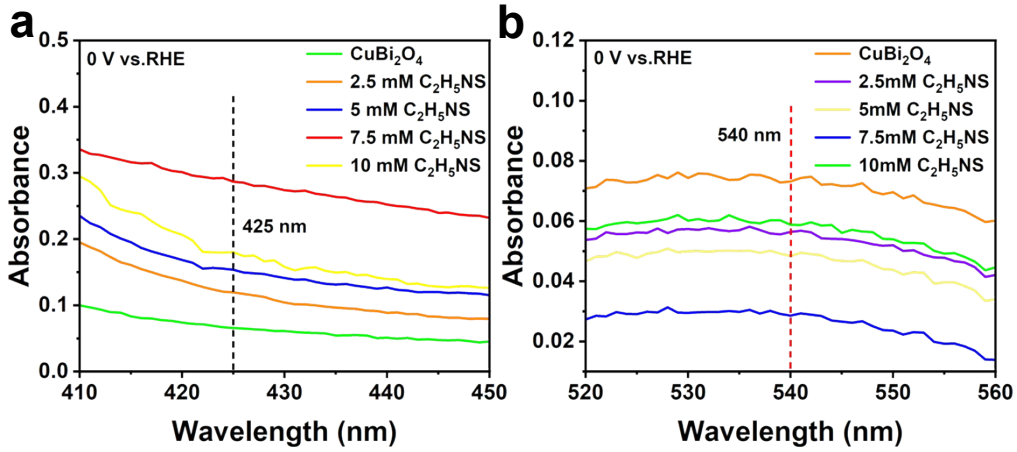

Fig. S22 UV-Vis absorption spectra of $CuBi_2O_4/Bi_2S_3$ with different quantity of sulfur sources: (a) NH_3 and (b) NO_2^- yield.

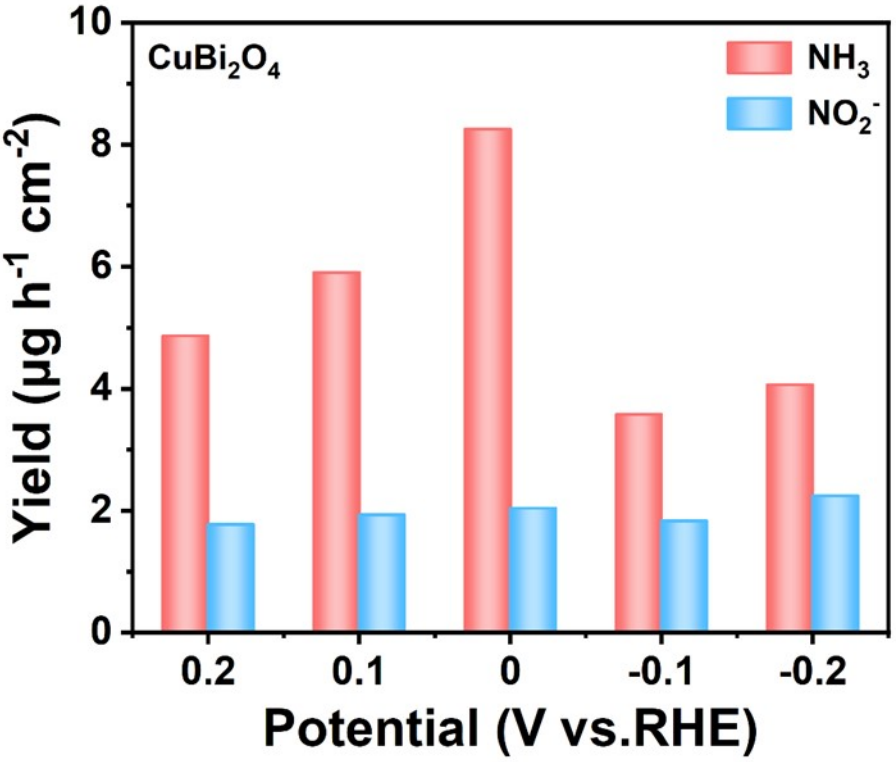

Fig. S23 NH_3 and NO_2^- yield of $CuBi_2O_4$ at different bias voltages.

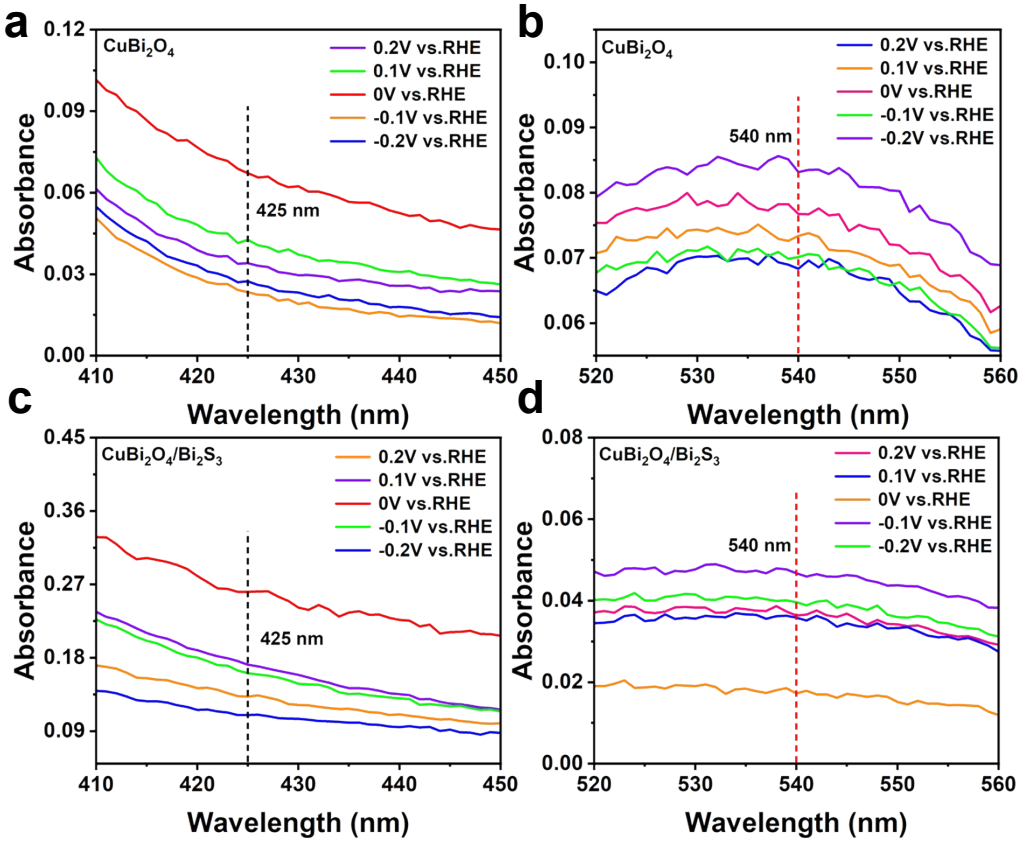

Fig. S24 UV-vis absorption spectra of $CuBi_2O_4$ at different photovoltages: (a) NH_3 and (b) NO_2^- yields rate. UV-vis absorption spectra of $CuBi_2O_4/Bi_2S_3$ at different photovoltages: (c) NH_3 and (d) NO_2^- yields rate.

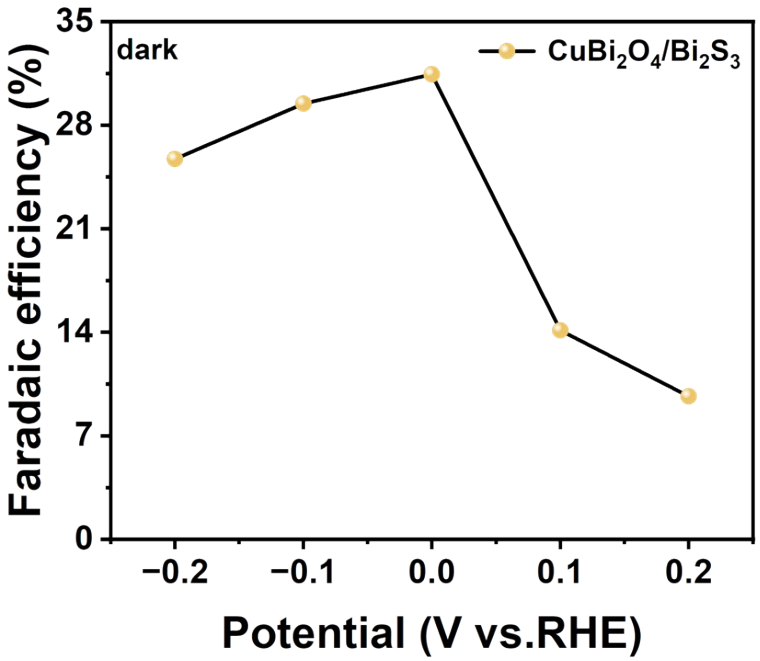

Fig. S25 FE_{NH3} of different bias voltages under dark condition.

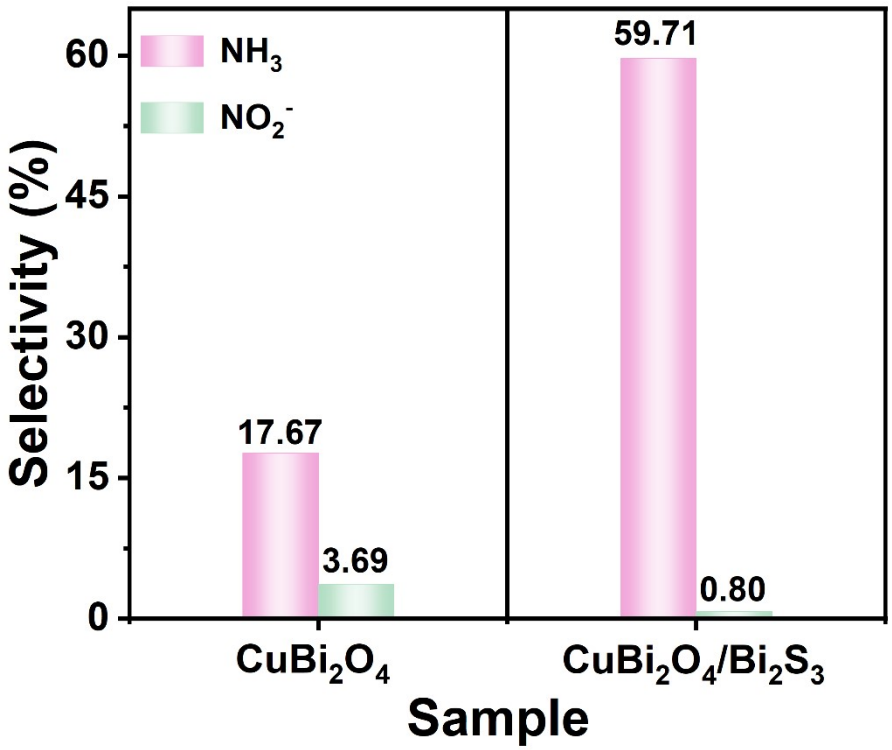

Fig. S26 NH_3 selectivity and NO_2^- selectivity of $CuBi_2O_4$ and $CuBi_2O_4/Bi_2S_3$.

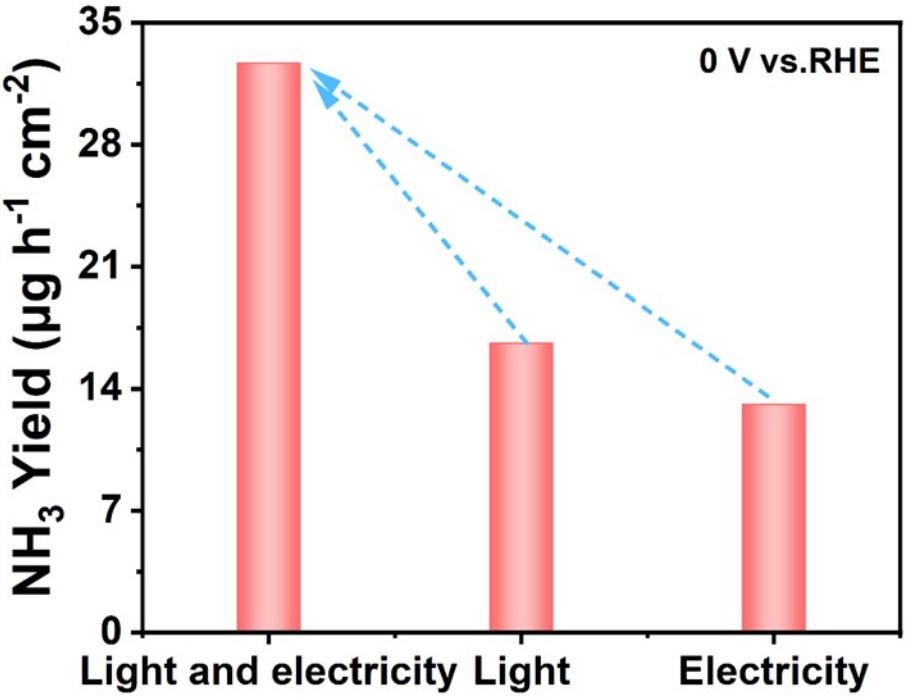

Fig. S27 NH_3 yield under different conditions of $CuBi_2O_4/Bi_2S_3$.

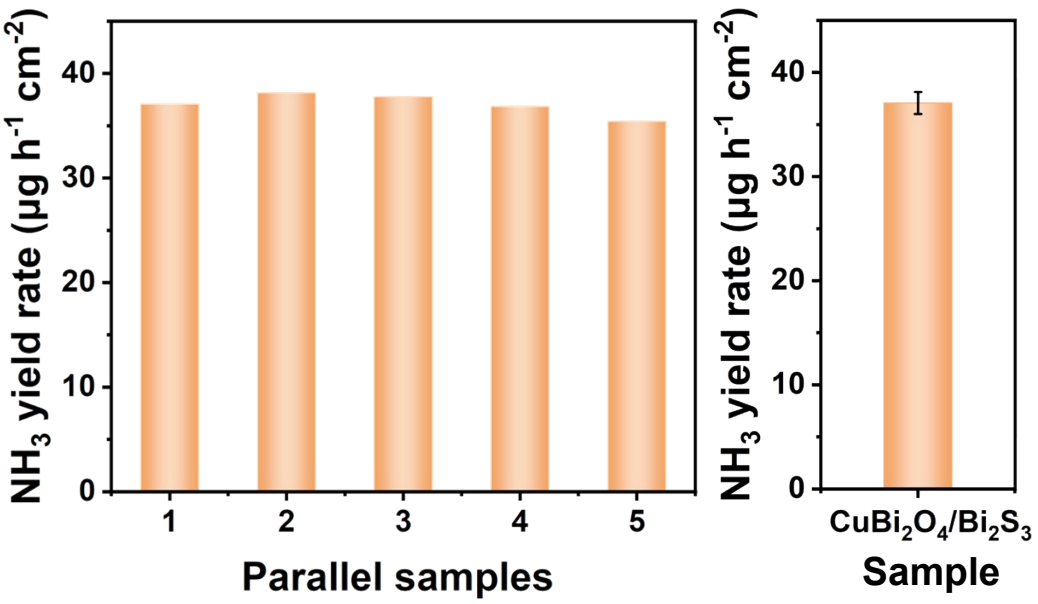

Fig. S28 NH_3 yield rate of $CuBi_2O_4/Bi_2S_3$ in NO_2^- reduction.